

**Assisting anti-PD-1 antibody treatment with a liposomal system capable of  
recruiting immune cells**

**Supplementary Data, including:**

**Supplementary Table;**

**Supplementary Figures.**

**Supplementary table 1. Primers for real time PCR**

Target	Forword primer (5'-3')	Reverse promoter (3'-5')
$\beta$ -actin	GGGAAATCGTGCGTGAC	AGGCTGGAAAAGAGCCT
CD8	CAAACACGCTTTCGGCTCCTG	CGGATTGGACTTCGCCTGTGA
Foxp3	GGCTCCTCTTCTTGCGAAACTC	TCACCTATGCCACCCTTATCCG
IL-4	CTTGGAAGCCCTACAGACGAG	TTGAACGAGGTCACAGGAGAA
TNF- $\alpha$	CTCCTCCACTTGGTGGTTTGT	CTCAAGTGGCATAGATGTGGA
IFN- $\gamma$	GACGCTTATGTTGTTGCTGAT	CTCAAGTGGCATAGATGTGGA
Hsp-70	GGCTGATCGGCCGCAAGTT	GGAAGGGCCAGTGCTTCAT

**Supplementary table 2. The mean diameter and zeta potential of different nanoparticles 9 month after**

Nanoparticles	Diameter (nm)	Zeta potential (mV)
P-nps	127.6 ± 0.9	-4.28 ± 1.18
N-nps	123.5 ± 0.5	-8.77 ± 1.49
FN-nps	134.6 ± 1.6	-7.13 ± 2.25

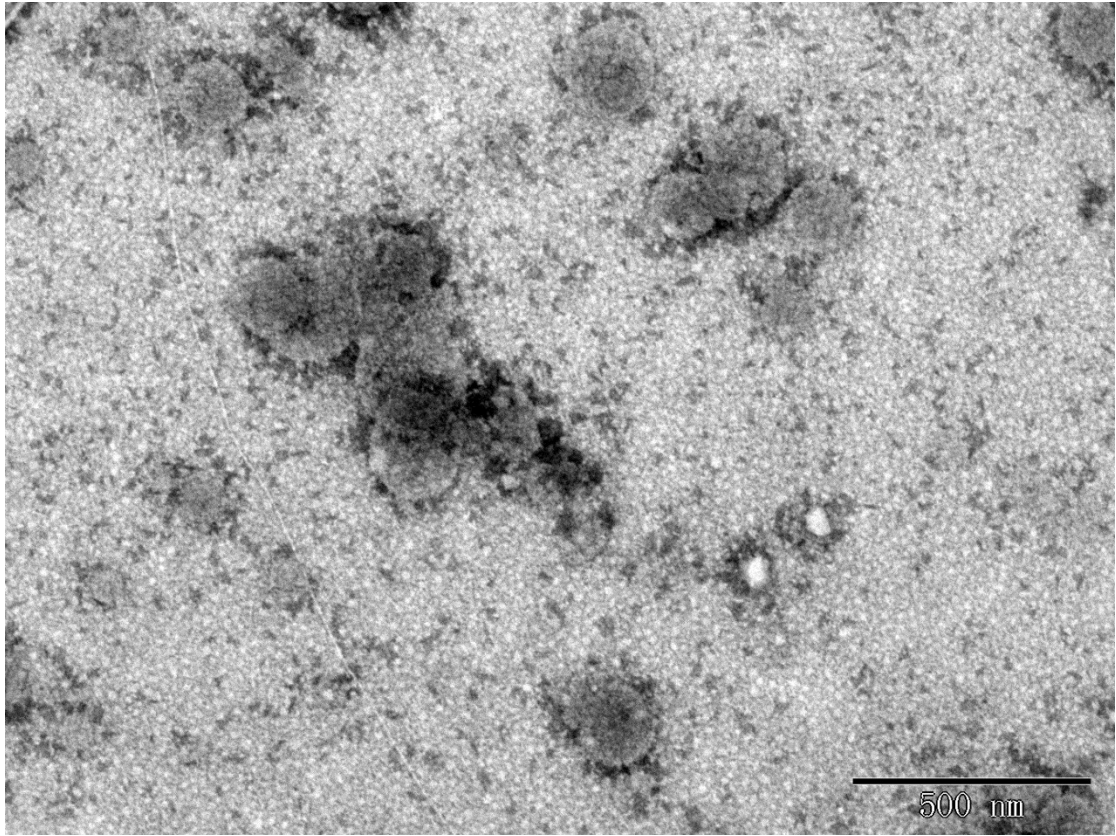


**Figure S1. Transmission electron microscopy (TEM) imaging of the FN-nps.**

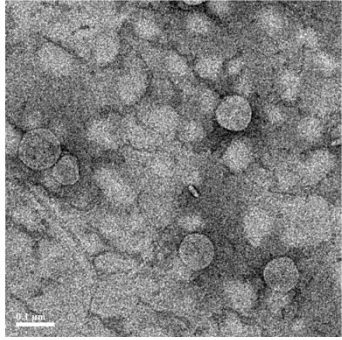


**Figure S2. Transmission electron microscopy (TEM) imaging of the FN-nps 9 months after.**

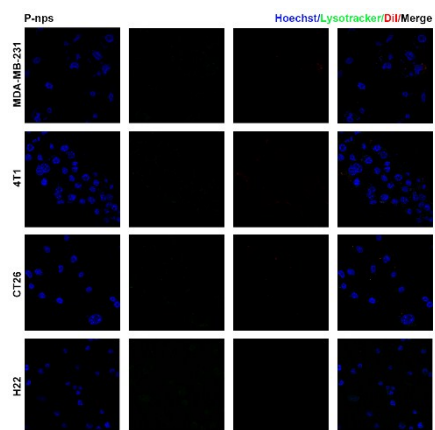


**Figure S3. Cellular uptake and intracellular trafficking of P-nps of H22, 4T1, CT26 and MDA-MB-231 cell lines.**

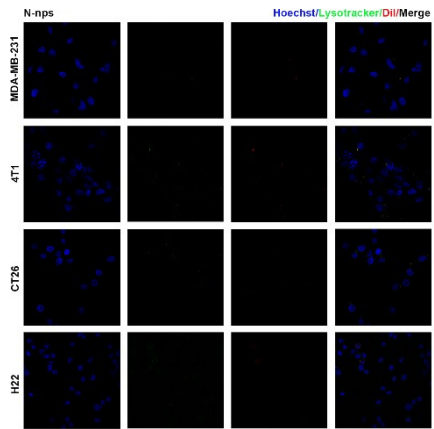


**Figure S4. Cellular uptake and intracellular trafficking of N-nps of H22, 4T1, CT26 and MDA-MB-231 cell lines.**

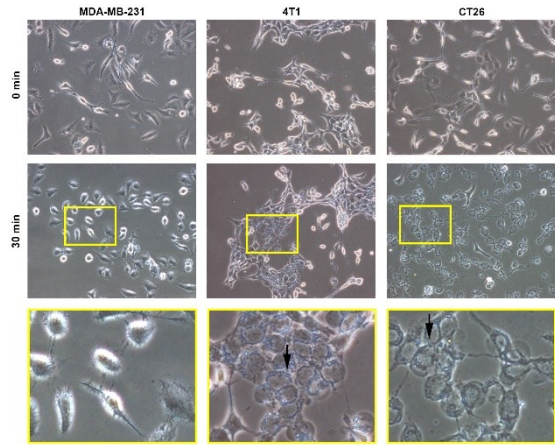


**Figure S5. Gas-generating ability of FN-nps *in vitro*.** The black arrows are pointing at the bubbles. Scale bar: 10  $\mu\text{m}$ .

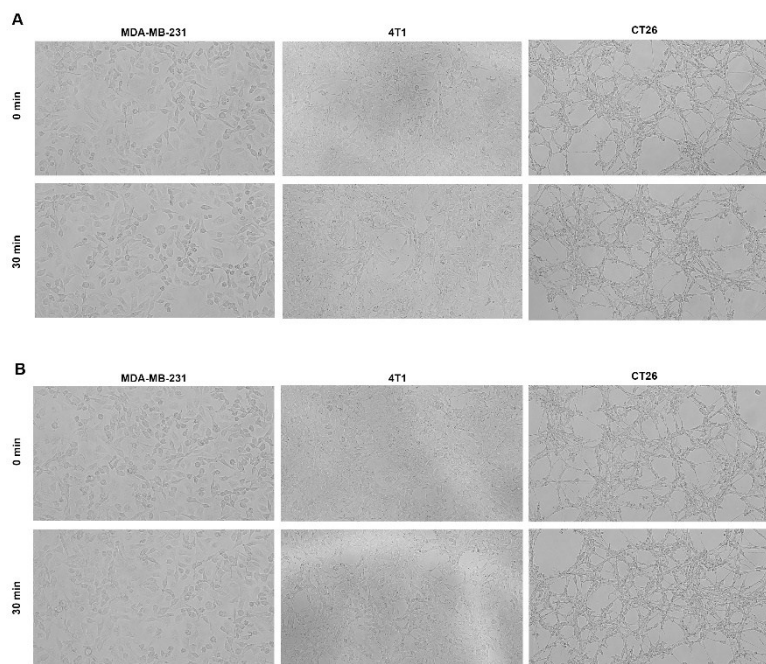


**Figure S6. Gas-generating ability of N-nps and P-nps *in vitro*.** (A) Gas-generating ability of N-nps. (B) Gas-generating ability of P-nps. Scale bar: 10  $\mu$ m.

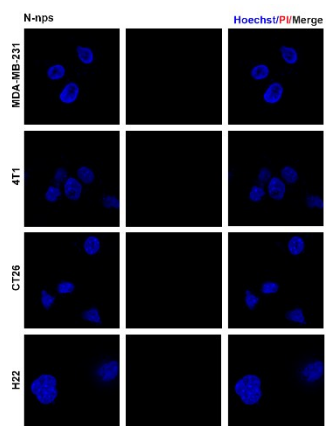


**Figure S7. CLSM images of H22, 4T1, CT26 and MDA-MB-231 cell lines after incubated with N-nps for 1h, then incubated with PI for 10min.**

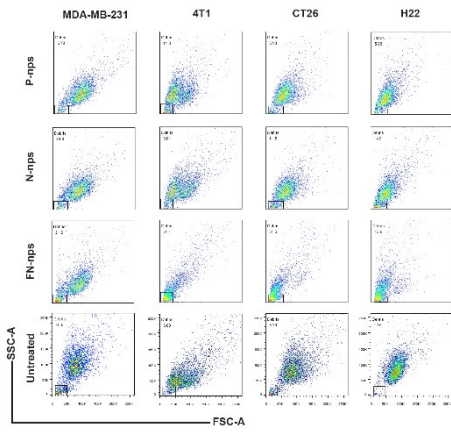


**Figure S8. Capability of generating debris of FN-nps, N-nps and P-nps in H22, 4T1, CT26 and MDA-MB-231 cell lines (n=3).**

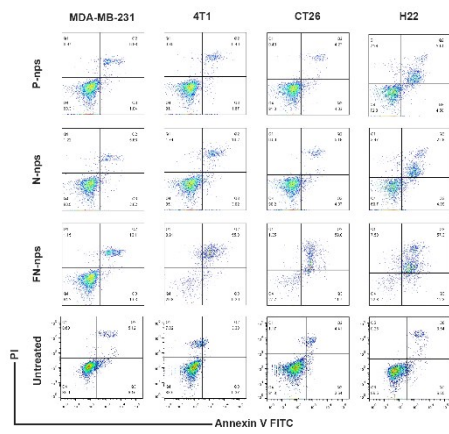


**Figure S9. Cell viability of FN-nps, N-nps and P-nps in H22, 4T1, CT26 and MDA-MB-231 cell lines (n=3).**

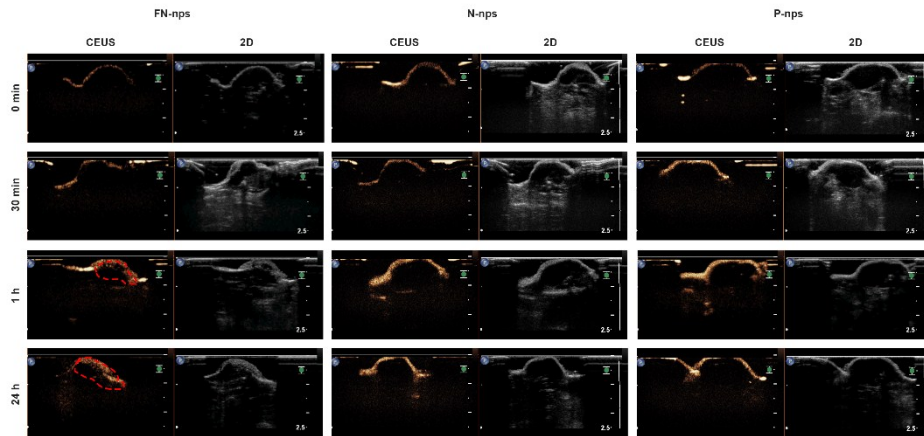


**Figure S10. Ultrasound imaging of the P-nps, N-nps and FN-nps *in vivo*.**

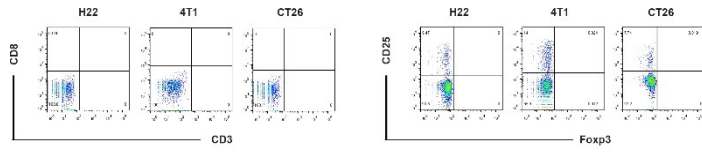


**Figure S11. The fluorescence minus one (FMO) controls of CTLs and Tregs in H22, 4T1 and CT26 tumor models.**

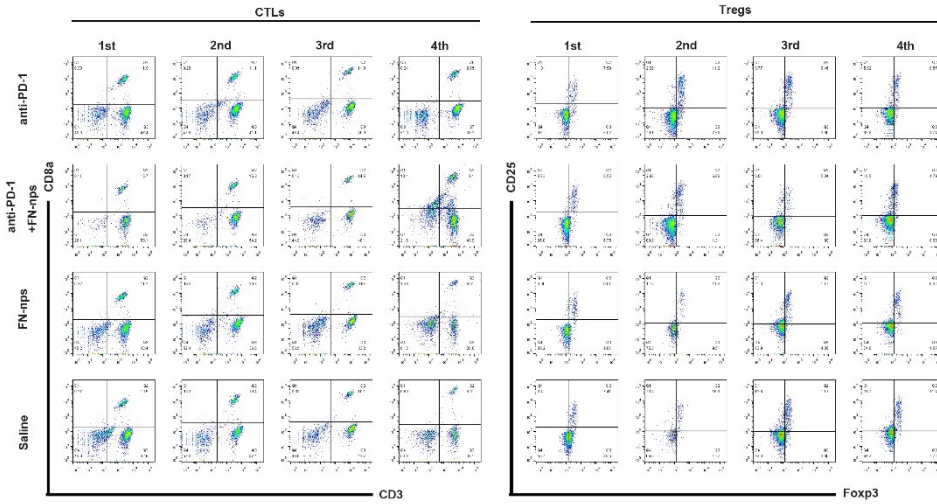


**Figure S12. The peripheral blood lymphocyte subsets of H22 tumor model after different administrations (n=3).**

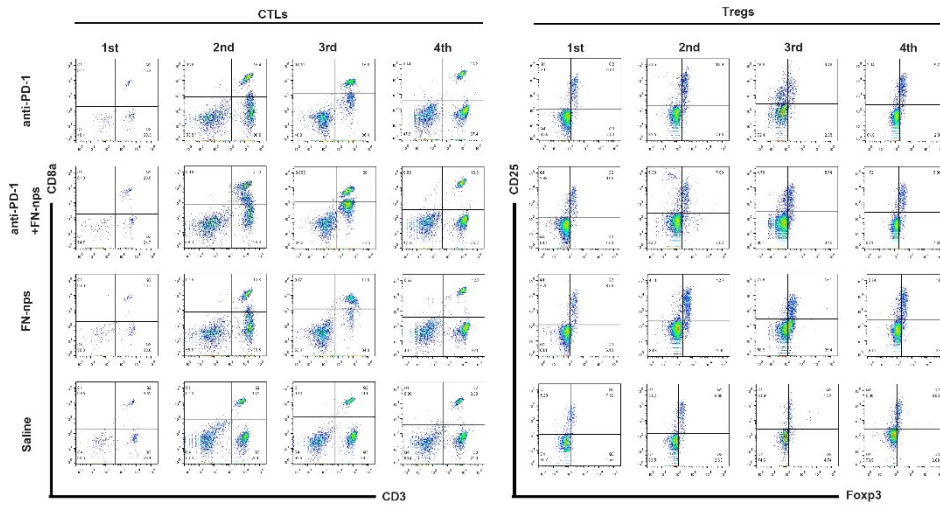


**Figure S13. The peripheral blood lymphocyte subsets of 4T1 tumor model after different administrations (n=3).**

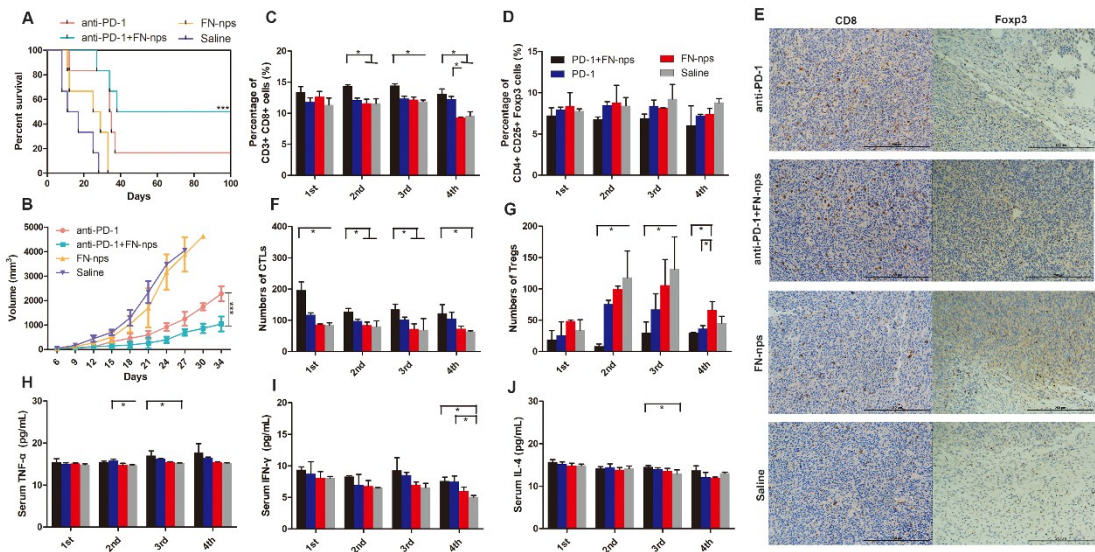


**Figure S14. The peripheral blood lymphocyte subsets of CT26 tumor model after different administrations (n=3).**

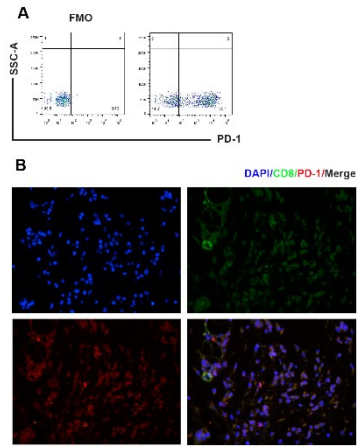


**Figure S15. The expression of PD-1 of CTLs.** (A) The expression of PD-1 of CD3+ CD8+ CTLs in PB. (B) The expression of PD-1 of CD8+ CTLs in tumor site.

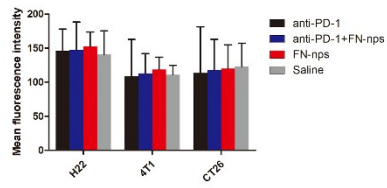
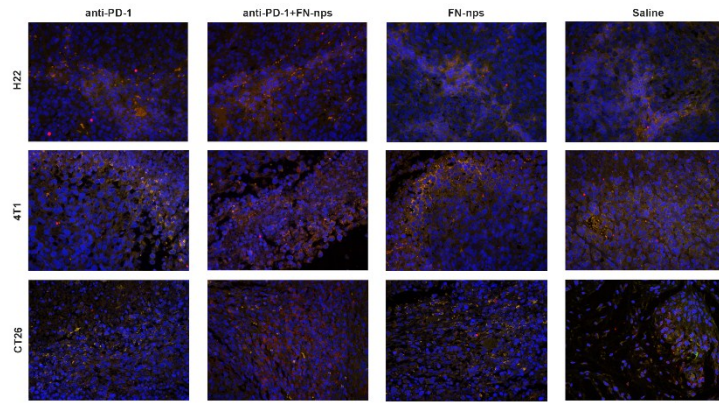


**Figure S16. The activation of DC in tumor site.** Data are expressed as the mean  $\pm$  sd (n=3).

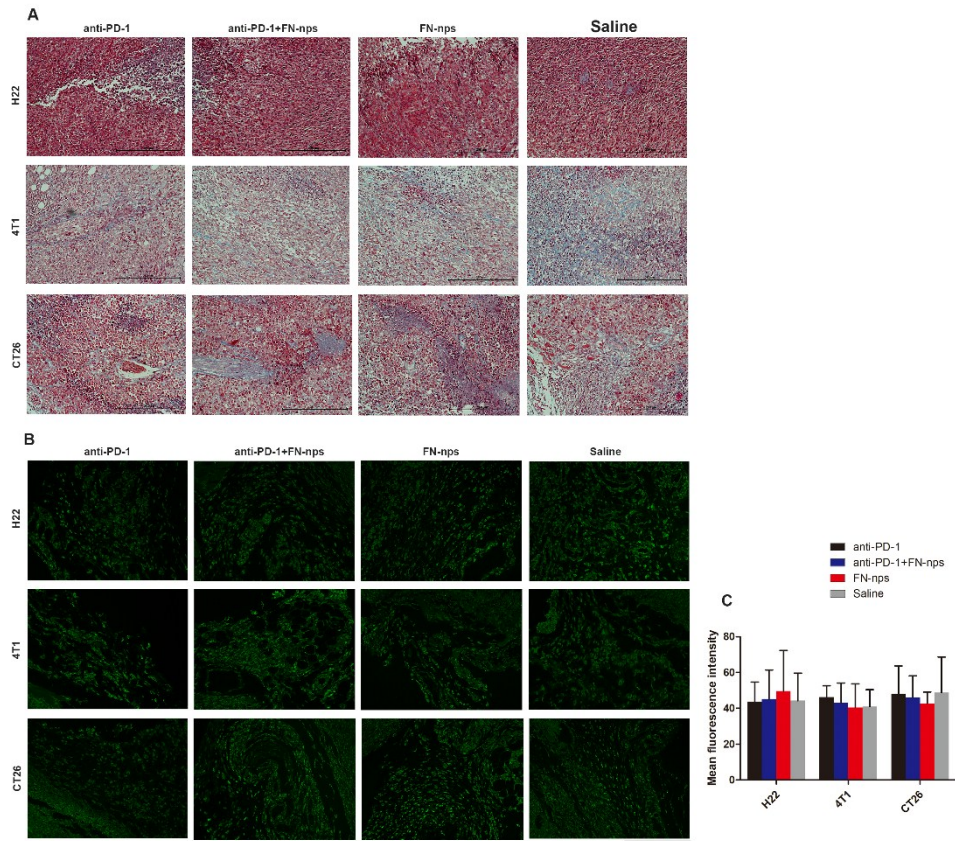


**Figure S17. The tumor microenvironment in the anti-PD-1, FN-nps, antiPD-1+FN-nps and saline groups.** (A) The desmoplastic structure of tumor. (B) The hypoxia level of tumor. (C) The mean fluorescence intensity data of hypoxia level. Data are expressed as the mean  $\pm$  sd (n=3).

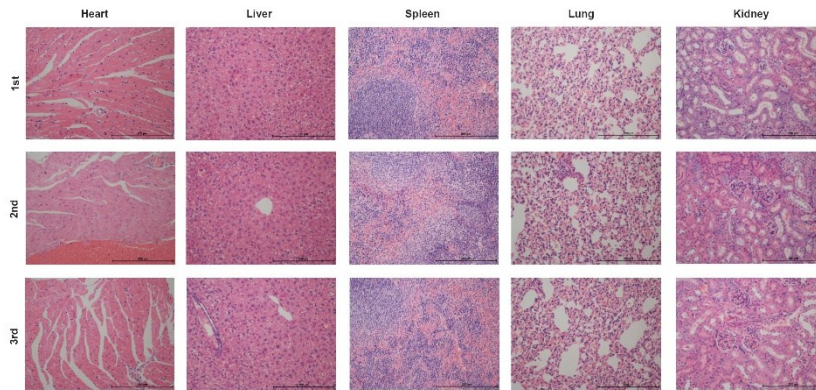


**Figure S18. Safety evaluation of anti-PD-1 antibody, the FN-nps and saline *in vivo* after 1<sup>st</sup>, 2<sup>nd</sup> and 3<sup>rd</sup> administration.** Each organ was sectioned for hematoxylin and eosin (H&E) staining. Scale bar, 250 μm.